

Novel hybrid nanocomposites of polyhedral Cu₂O nanoparticles–CuO nanowires with enhanced photoactivity

Cite this: *Phys. Chem. Chem. Phys.*, 2014, **16**, 17487

Chao Wang,^a Yiqian Wang,^{*ab} Xuehua Liu,^a Feiyu Diao,^a Lu Yuan^c and Guangwen Zhou^c

Novel hybrid nanocomposites of Cu₂O nanoparticles (NPs) partially embedded in CuO nanowires (NWs) were produced by simple thermal reduction of CuO NWs in a vacuum. It is found that most Cu₂O NPs adopt two regular shapes, one being cubic and the other being octahedral. The shape selection of the Cu₂O nanocrystals is governed by the orientation relationship between Cu₂O NPs and CuO NWs. The formation of such hierarchical hybrid nanostructures is induced by the topotactic reduction of CuO NWs. Compared with pure CuO NWs, the polyhedral Cu₂O NP–CuO NW hierarchical hybrid nanostructures exhibit enhanced ability to photodegrade methyl orange under visible light, which is attributed to the synergic effects of CuO NWs and Cu₂O NPs.

Received 18th April 2014,
Accepted 7th July 2014

DOI: 10.1039/c4cp01696c

www.rsc.org/pccp

Introduction

Hybrid nanocomposites composed of two or more nanomaterials are usually designed to improve their performance over individual components. The hybrid nanocomposites with well-defined building blocks, narrow size distributions and tailorable physical or chemical properties have demonstrated huge potential in a wide range of application fields, such as photoelectrochemical devices,^{1,2} ultrasensitive detection,³ lithium-ion batteries,^{4,5} and heterogeneous catalysis.^{6,7} As an important semiconductor oxide, CuO possesses a narrow band-gap of 1.2–1.9 eV and large photoconductivity. To further improve the physical and chemical properties of CuO nanomaterials, considerable effort has been directed towards the synthesis of CuO–CeO₂,⁸ CuO–ZnO,^{9,10} CuO–TiO₂¹¹ and CuO–TiO_{2-x}N_x¹² hybrid nanocomposites. However, these hybrid nanocomposites lack good orientation relationship between different components, and the microstructure of these hybrid interfaces has not yet been investigated in detail. As we all know crystal facets can greatly influence the photocatalytic activities. For Cu₂O, {111} facets have better photocatalytic activity compared to {100} facets.¹³ The facets of Cu₂O nanoparticles are determined by the orientation relationship between Cu₂O nanoparticles and CuO

nanowires. Therefore, the orientation relationship can play an important role in the photocatalytic activity.

CuO nanowires (NWs) can be synthesized by various methods, for example, thermal oxidation of copper foil in an oxygen atmosphere,¹⁴ aqueous reaction¹⁵ and hydrothermal methods.¹⁶ From a thermochemical viewpoint,¹⁷ CuO is unstable under the conditions of very low oxygen pressure and high temperature, where a reduction reaction of $4\text{CuO(s)} \rightarrow 2\text{Cu}_2\text{O(s)} + \text{O}_2\text{(g)}$ can take place. Therefore, novel Cu₂O–CuO hybrid nanocomposites can be achieved through the direct reduction of CuO NWs in a vacuum.

In this paper, we report novel hierarchical hybrid nanocomposites of polyhedral Cu₂O nanoparticles (NPs)–CuO NWs prepared by thermal reduction of CuO NWs. Extensive transmission electron microscopy (TEM) observations demonstrate that Cu₂O NPs possess a cubic or octahedral shape, depending on their orientation relationship with the parent CuO NWs. Compared with pure CuO NWs, the Cu₂O NP–CuO NW hybrid nanostructures show enhanced photocatalytic activity, which is attributed to the synergic effects of CuO NWs and Cu₂O NPs.

Experimental

A two-step process, oxidation of copper foil and reduction of CuO NWs, is involved in our experiment. CuO NWs can be prepared by heating a Cu foil (polycrystalline foil, 99.99% purity, obtained from Sigma-Aldrich) in air¹⁸ or in a vacuum chamber filled with oxygen gas.^{19,20} In our case, the Cu foil was oxidized for 2 h at an oxygen pressure of 200 Torr and 450 °C to grow CuO NWs. This procedure yields well-aligned CuO NWs

^a The Cultivation Base for State Key Laboratory, Qingdao University, No. 308 Ningxia Road, Qingdao 266071, People's Republic of China. E-mail: yqwang@qdu.edu.cn; Tel: +86-532-83780318

^b College of Physics, Qingdao University, No. 308 Ningxia Road, Qingdao, 266071, People's Republic of China

^c Department of Mechanical Engineering & Multidisciplinary Program in Materials Science and Engineering, State University of New York, Binghamton, NY 13902, USA

perpendicular to the Cu foil, and CuO NWs are grown on both surfaces of the oxidized Cu foil. To prepare Cu₂O NP–CuO NW hybrid nanostructures, the oxidized Cu foils were directly annealed at 450 °C in the same chamber under the vacuum of $\sim 2 \times 10^{-6}$ Torr and then cooled down to room temperature in a vacuum.

The morphologies and microstructures of the oxidized and reduced samples were examined using a field emission gun scanning electron microscope (FEG-SEM, FEI Supra 55VP) and a transmission electron microscope (TEM, JEOL JEM2100F) operated at 200 kV. Electron energy-loss spectroscopy (EELS) analysis was performed on a Tecnai F20 TEM.

To compare the photocatalytic activities of Cu₂O NP–CuO NW nanocomposites and pure CuO NWs, all the photocatalysis tests were performed under the same experimental conditions. The visible light photodegradation experiments were carried out in a 100 mL glass bottle using methyl orange (MO) solution as a photocatalytic dye. Typically, 10 mg of the test sample was suspended in a 50 mL aqueous solution of MO (20 mg L⁻¹) to form a suspension. Small pieces of glass were used to scrape off the test samples from the Cu foils. The small pieces of glass were then put into the aqueous solution of MO. The weight of test samples for the photodegradation experiments was determined through measuring the weight loss of Cu foils before and after the scraping. The suspension was magnetically stirred in the dark for 3 h to ensure the establishment of an adsorption–desorption equilibrium of the dye on the sample surface before being irradiated by a 500 W xenon lamp equipped with an ultraviolet (UV) cutoff filter ($\lambda > 380$ nm). Upon turning on the light, air was continuously introduced into the aqueous solution at a flow rate of ~ 20 sccm. At given irradiation time intervals, 2 mL of the reaction suspension was taken out, and then separated by centrifugation for 3 min at a rotational speed of 3000 rpm. At the beginning, the time interval is 15 min, and is increased to 30 min after 30 minute photocatalytic degradation. The MO concentration was determined by monitoring the height of absorbance maximum in UV-vis absorption spectra (MO at 464 nm), which were recorded on a TU 1909 UV-vis spectrophotometer.

Results and discussion

Fig. 1a shows a representative scanning electron microscopy (SEM) image of NWs formed after the oxidation of a Cu foil. The NWs have lengths up to several microns with an average length of ~ 4 μm and a relatively uniform diameter of ~ 100 nm. Fig. 1b presents a zoom-in SEM image of a single nanowire (NW), showing that the NW has a smooth surface. Fig. 1c shows a typical SEM image of NWs after being annealed in a vacuum at 450 °C for 2 h. The initially straight and smooth NWs become a little curved with significantly increased surface roughness. Some of the reduced NWs show saw-toothed surface morphology. As revealed by a zoom-in SEM image shown in Fig. 1d, the NW surface is covered with a high density of NPs.

To verify the chemical composition of the NWs and NPs after the reduction process, EELS analysis was performed on the

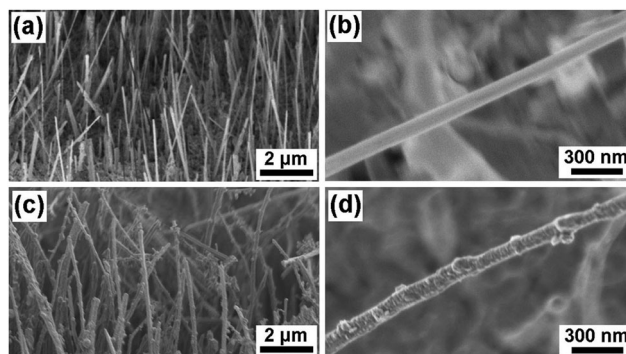


Fig. 1 Morphologies of the NWs before and after thermal reduction. (a) SEM image of the NWs before thermal reduction; (b) zoom-in SEM image of a single nanowire before reduction; (c) SEM image of the NWs after reduction in a vacuum at 400 °C for 2 h; and (d) zoom-in SEM image of the reduced NWs.

NWs and NPs, respectively. Fig. 2a shows a representative bright-field (BF) TEM image of a single NW reduced in a vacuum at 450 °C for 1 h, on which three NPs can be clearly seen. Fig. 2b–e show the EELS spectra obtained from an individual nanoparticle (NP) and the NW in Fig. 2a, respectively. All the EELS spectra are first background subtracted and then deconvoluted to remove the plural scattering. Subsequently, the atomic ratio of Cu and O can be quantified through calculating the peak intensities of Cu–L_{2,3} and O–K edges. Quantification results for the NW show that the ratio of Cu:O is very close to 1:1, suggesting that it has a chemical formula of CuO. However, quantification results for the NPs demonstrate that the ratio of

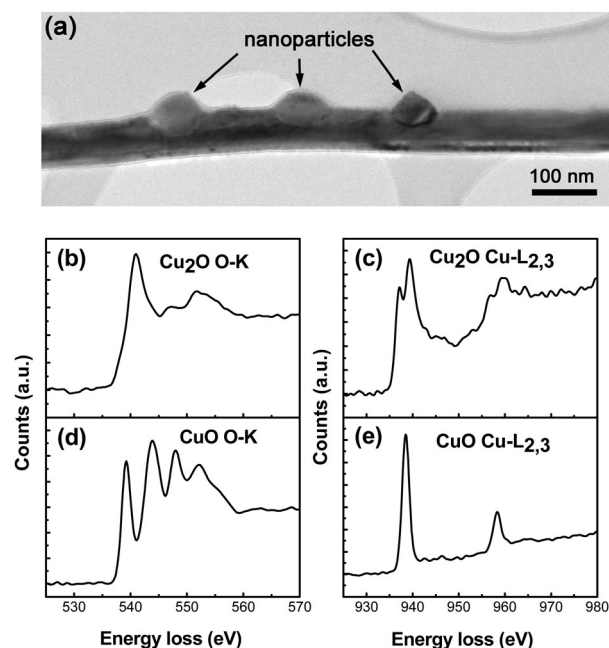


Fig. 2 Chemical composition and electronic structure analysis of the NP–NW hybrid nanostructure. (a) BF TEM image of a single NW decorated with NPs; EELS spectra of O–K and Cu–L_{2,3} edges obtained from the NPs (b and c) and NWs (d and e).

Cu:O is $2 \pm 0.06:1$, indicating that the NP is Cu_2O . Careful examination of the EELS spectra shows that there are remarkable differences in the O–K edge fine structures of the NPs and NWs. In the EELS spectrum (Fig. 2b) of the NPs a sharp peak at 539 eV and a diffuse hump at 552 eV can be seen, whereas in the EELS spectrum (Fig. 2c) of the NWs four peaks appear, which are separated by 5, 4 and 5 eV. The Cu– L_2 edges of both NPs and NWs show a strong “white line” (939 eV). However, the Cu– L_3 edges of NPs show a weaker ionization edge compared with that of the NW (Fig. 2d and e).

The particular electronic structures of the copper oxides are different, due to their different atomic coordination and chemical bonding. In the compound CuO, some 3d electrons are drawn away from the neighborhood of the copper nucleus, leading to a much larger possibility of L_2 , L_3 transitions, and sharp L_2 , L_3 “white lines” appear.^{21–23} As for Cu_2O , fewer 3d electrons are drawn away from copper atoms; some 3d vacancies are still available for L_2 , L_3 transitions, and L_2 , L_3 “white lines” thus appear with less sharpness, as reported in the previous study.²¹

To clarify the orientation relationship between Cu_2O NPs and CuO NWs, extensive TEM examination was carried out on individual NWs dispersed onto a holey-carbon-film-coated copper grid. It shows that most of the Cu_2O NPs on the CuO NWs have two dominant regular shapes, one being cubic and the other being octahedral. To give a reliable occurrence frequency for different shapes of Cu_2O NPs, more than 100 individual CuO NWs decorated with Cu_2O NPs are examined, and a statistical analysis is carried out. It shows that cubic Cu_2O NPs have a volume fraction of nearly 20% while octahedral Cu_2O NPs have a volume fraction of around 80%. In addition, it is found that cubic Cu_2O NPs grow on the surface of CuO NWs with an epitaxial orientation relationship of $[001]_{\text{CuO}}//[001]_{\text{Cu}_2\text{O}}$, $\{110\}_{\text{CuO}}//\{220\}_{\text{Cu}_2\text{O}}$. However, octahedral Cu_2O NPs prefer to grow with an epitaxial orientation relationship of $[001]_{\text{CuO}}//[110]_{\text{Cu}_2\text{O}}$, $\{\bar{1}10\}_{\text{CuO}}//\{111\}_{\text{Cu}_2\text{O}}$.

Fig. 3a shows an example of a cubic Cu_2O NP–CuO NW hybrid nanostructure. In the SAED pattern (Fig. 3b) two sets of diffraction patterns are visible. One labeled by red lines matches well with the crystal structure of CuO along the $[001]$ zone axis and the other marked by yellow lines can be indexed well with the Cu_2O structure along the $[001]$ zone axis. Therefore the orientation relationship between the CuO NW parent and the Cu_2O NPs is determined to be $[001]_{\text{CuO}}//[001]_{\text{Cu}_2\text{O}}$, $\{110\}_{\text{CuO}}//\{220\}_{\text{Cu}_2\text{O}}$. Fig. 3c shows a typical $[001]$ zone-axis high-resolution transmission electron microscopy (HRTEM) image from the Cu_2O NPs edge as marked by a black rectangle A in Fig. 3a, which reveals that the facet of the Cu_2O NPs is $\{200\}$. So the shape of NPs is determined to be a cube, which is bounded by six $\{200\}$ surfaces.²⁴ Fig. 3d is a HRTEM image from the interface area between CuO NWs and Cu_2O NPs as indicated by a black square B in Fig. 3a. The CuO/ Cu_2O interface formed by the oxide reduction is clearly visible, where misfit dislocations can be seen. Fig. 3e shows the one dimensional Fourier-filtered lattice image of the white rectangle in Fig. 3d. It can be seen clearly that one in seven extra half plane is inserted vertically.

Fig. 4a shows an example of an octahedral Cu_2O NP–CuO NW hybrid nanostructure. The facet of the Cu_2O NPs is $\{111\}$

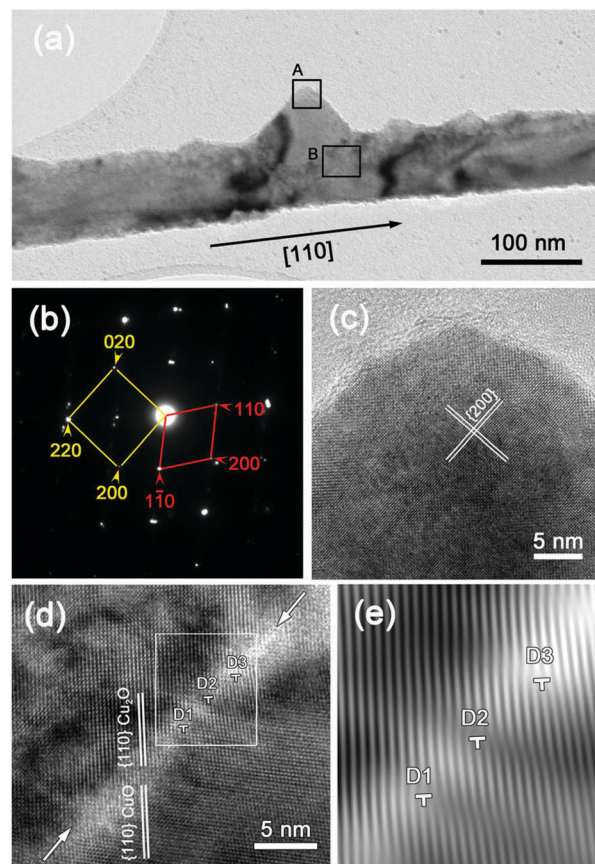


Fig. 3 An example of a cubic Cu_2O NP–CuO NW hybrid nanostructure. (a) BF TEM image; (b) SAED pattern; (c) HRTEM image of rectangular region A in (a); (d) HRTEM image of rectangular region B in (a); and (e) Fourier-filtered HRTEM image of the rectangular region in (d).

determined by the HRTEM image (Fig. 4d) and the angle between two facets of the NPs is about 70.5° measured from Fig. 4b, which matches the angle between $\{111\}$ facets of the face-centered cubic. Therefore the shape of Cu_2O is octahedral.²⁴ Fig. 4c is the SAED pattern obtained from the NP–NW interface region: one matches well with the crystal structure of CuO along the $[001]$ zone axis marked by red lines and the other can be indexed well with the Cu_2O structure along the $[110]$ zone axis labeled by yellow lines. The orientation relationship between the Cu_2O NPs and the parent CuO NWs identified from the diffraction patterns is thus $[001]_{\text{CuO}}//[110]_{\text{Cu}_2\text{O}}$, $\{\bar{1}10\}_{\text{CuO}}//\{111\}_{\text{Cu}_2\text{O}}$. Fig. 4e is an HRTEM image from the Cu_2O /CuO interface area as indicated by a black square in Fig. 4b, where the orientation at the interface matches with the SAED pattern shown in Fig. 4c.

Fig. 5 shows another example of an octahedral Cu_2O NP–CuO NW hybrid nanostructure. Obviously, the Cu_2O NPs rotates 90° around the zone axis compared with the Cu_2O NPs in Fig. 4. However, the growth direction of the CuO NW also whirls 90° in the meantime. Therefore, the orientation relationship between the Cu_2O NPs and the CuO is still $[001]_{\text{CuO}}//[110]_{\text{Cu}_2\text{O}}$, $\{\bar{1}10\}_{\text{CuO}}//\{111\}_{\text{Cu}_2\text{O}}$, which can be confirmed by the SAED in Fig. 5b and HRTEM in Fig. 5c.

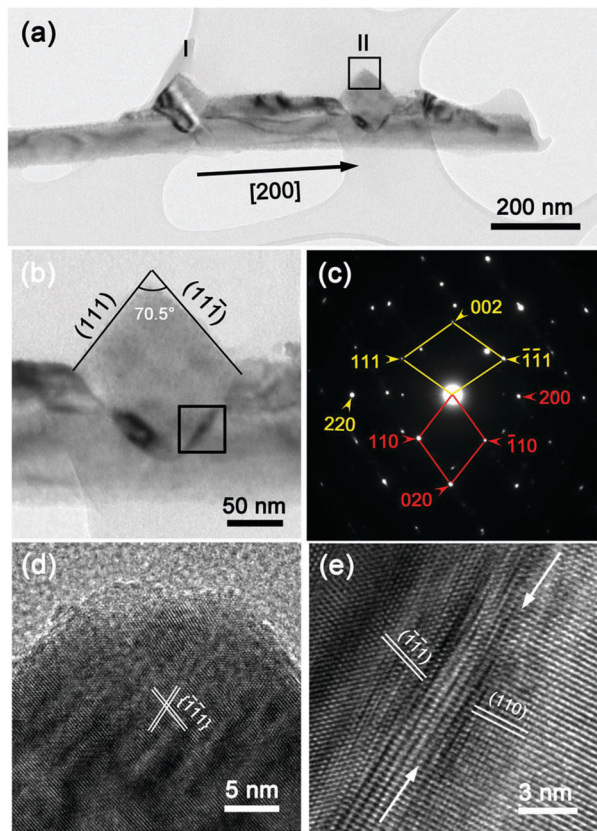


Fig. 4 An example of an octahedral Cu_2O NP–CuO NW hybrid nanostructure. (a) BF-TEM image; (b) zoom-in BF-TEM image of the Cu_2O NPs; (c) SAED pattern obtained from the hybrid nanostructures; (d) HRTEM image of the rectangular region in (a); and (e) HRTEM image of the rectangular region in (b).

Reduction through the dissociation of CuO oxide can be described by the reaction $4\text{CuO}(\text{s}) \rightarrow 2\text{Cu}_2\text{O}(\text{s}) + \text{O}_2(\text{g})$. Interestingly, only cubic and octahedral Cu_2O NPs were found on the surfaces of CuO NWs after the reduction process. Based on the experimental results, a formation mechanism was proposed. Firstly the Cu_2O nucleation process occurs in the regions with impurity atoms or dislocations, where the surface energy is relatively high.²⁵ Low pressure of O_2 and high temperature will lead to the generation of oxygen vacancies in these regions, which induce a substantial increase in the length of the b -axis, with a reduction in the length of a and c axes.¹⁷ When removing sufficient oxygen atoms in an ordered way (or *via* ordering of oxygen vacancies), a hybrid structure will form, in which the rearrangement of atoms can lead to Cu_2O formation with the corresponding modification of the unit cell. After the nucleation process, oxygen atoms move along the $\text{Cu}_2\text{O}/\text{CuO}$ interface to the surface of CuO NWs, in the meantime Cu_2O NPs grow with the identified crystallographic orientation relationships. The reduction process is schematically shown in Fig. 6. The shape of the Cu_2O nanocrystal is determined in the nucleation stage. CuO adopts a monoclinic structure with a space group of $C2/c$, in which each copper atom is bonded to four oxygen atoms. After removing enough oxygen atoms in an ordered way, CuO tends to transform into Cu_2O with certain

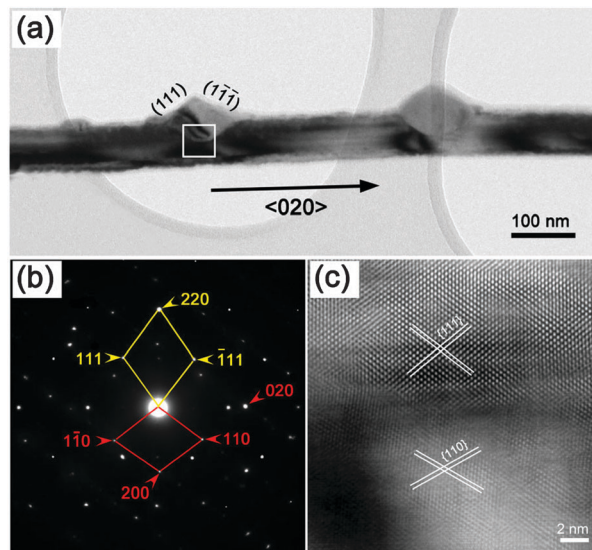


Fig. 5 An example of another octahedral Cu_2O NP–CuO NW hybrid nanostructure. (a) BF-TEM image; (b) SAED pattern; and (c) HRTEM image of the rectangular region in (a).

orientation relationships, which can result in a small lattice mismatch. Thus, the shape of Cu_2O is related to the orientation relationship between CuO NWs and Cu_2O NPs. From our observation, cubic Cu_2O NPs form on the surface of CuO NWs with an orientation relationship of $[001]_{\text{CuO}}//[001]_{\text{Cu}_2\text{O}}$, $\{110\}_{\text{CuO}}//\{220\}_{\text{Cu}_2\text{O}}$ and octahedral Cu_2O NPs grow on the surface of CuO NWs with an orientation relationship of $[001]_{\text{CuO}}//[110]_{\text{Cu}_2\text{O}}$, $\{1\bar{1}0\}_{\text{CuO}}//\{111\}_{\text{Cu}_2\text{O}}$. The Cu_2O NPs grow with cubic or octahedral shapes until they completely penetrate through

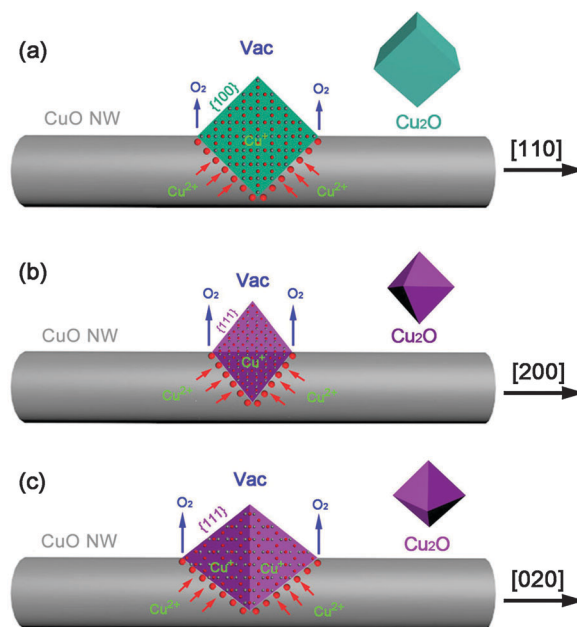


Fig. 6 Schematic illustration of topotactic formation mechanism for polyhedral Cu_2O NPs embedded in reduced CuO NWs. (a) CuO NWs with cubic Cu_2O NPs; (b) and (c) CuO NWs decorated with octahedral Cu_2O NPs.

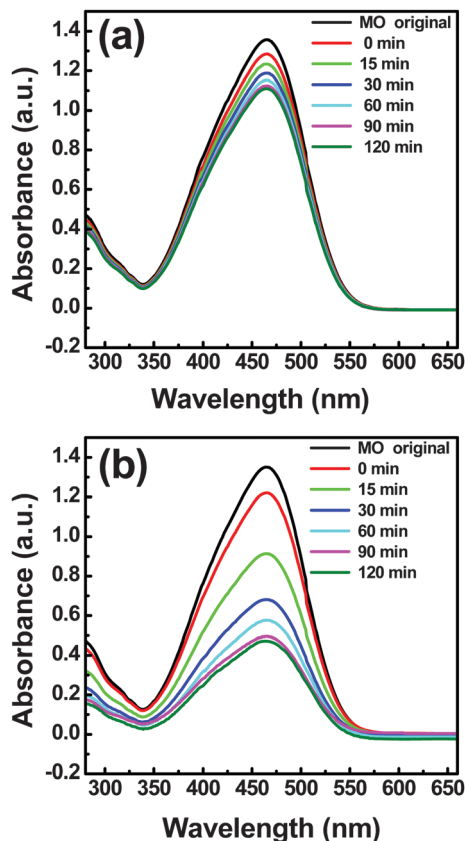


Fig. 7 UV-vis absorption spectra of an aqueous solution of MO in the presence of CuO NWs (a) and Cu₂O NPs-CuO NWs hybrid nanostructures (b).

the NW along the diameter direction, which was confirmed by the *in situ* TEM observations.²⁶

Fig. 7 shows the UV-vis absorption spectra of an aqueous solution of MO photodegraded by CuO NWs and Cu₂O NP-CuO NW hybrid nanostructures, respectively. All the photodegradation tests were carried out under visible light with air introduced into the aqueous solution of MO. The photocatalytic efficiency η can be calculated from the peak values in the UV-visible absorption spectra according to the following equation,

$$\eta = \frac{A_0 - A}{A_0} \times 100\% \quad (1)$$

where A_0 and A are the absorbance peak values without and with visible light for 2 h irradiation respectively. Based on the experimental results, the photocatalytic efficiency of pure CuO NWs and hybrid nanostructures is calculated to be 13.7% and 67.1% respectively. Therefore, the hybrid nanostructures exhibit much better ability to photodegrade MO compared to pure CuO NWs. In previous studies,^{27,28} CuO or Cu₂O nanomaterials demonstrated weak ability to photodegrade MO in the absence of H₂O₂. However, in our case, no H₂O₂ but only air was introduced into the aqueous solution.

To account for the enhanced photocatalytic activity of Cu₂O NP-CuO NW hybrid nanostructures, a possible photodegradation mechanism is proposed, which is schematically shown in Fig. 8. Under the visible light illumination, O₂ is first reduced to form

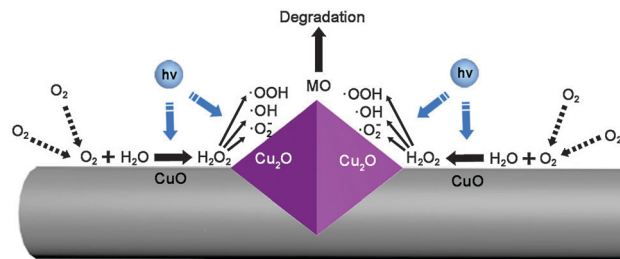
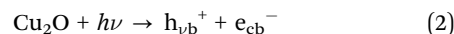
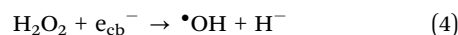


Fig. 8 The schematic illustration of the photodegradation mechanism for the enhanced photocatalytic activity of Cu₂O NP-CuO NW hybrid nanostructures.

H₂O₂ at the solid-liquid interface between CuO NWs and aqueous solution.²⁹ Meanwhile, Cu₂O NPs are excited to produce electrons and holes,²⁷ as shown in eqn (2):



Then the photo-generated electrons and holes initiate a series of photodegradation reactions, as shown below.²⁷ Finally, the azo group in MO is attacked by the oxidant species such as •OOH, •OH, and •O₂.³⁰



For Cu₂O NP-CuO NW hybrid nanostructures, O₂ is stored as H₂O₂ mediated by CuO NWs during the photodegradation process, and the oxidants are produced by the photodecomposition of H₂O₂ over Cu₂O. Therefore, the photocatalytic dye of MO can be degraded more efficiently, even without adding H₂O₂ into the solution. For the pure CuO NWs, although they can reduce O₂ to form H₂O₂ under visible light irradiation, the oxidant concentration is very low in the absence of Cu₂O NPs, which leads to very weak degradation of MO. So it can be deduced that the enhanced photocatalytic activity of the hybrid nanostructures originates from the synergic effects of CuO NWs and Cu₂O NPs. Our results provide a novel strategy for fabrication of hybrid nanocomposites with enhanced photocatalytic activities.

Conclusions

In summary, novel hybrid nanocomposite of polyhedral Cu₂O NPs-CuO NWs were produced by simple efficient thermal reduction of CuO NWs in a vacuum. The parent CuO NWs serve as the skeleton and the lower oxide of the Cu₂O phase resulting from the CuO reduction forms cubic or octahedral NPs on the parent CuO NWs. Cubic Cu₂O NPs form on the surface of CuO NWs with an orientation relationship of [001]_{CuO}//[001]_{Cu₂O}, {110}_{CuO}//{220}_{Cu₂O}. However, octahedral Cu₂O NPs grow on the surface of CuO NWs with an orientation relationship of [001]_{CuO}//[110]_{Cu₂O}, {110}_{CuO}//{111}_{Cu₂O}. Compared with pure CuO NWs, these hybrid nanostructures exhibit enhanced ability to photodegrade MO under visible light.

Acknowledgements

The work is financially supported by National Key Basic Research Development Program of China (grant no. 2012CB722705), the Natural Science Foundation for Outstanding Young Scientists in Shandong Province, China (grant no. JQ201002), and the Program for Foreign Cultural and Educational Experts (grant no. W20123702083, GDW20123702162). Y. Q. Wang would like to thank the financial support from the Top-notch Innovative Talent Program of Qingdao City and the Taishan Scholar Program of Shandong Province, China.

References

- 1 G. Ghadimkhani, N. R. de Tacconi, W. Chanmanee, C. Janaky and K. Rajeshwar, *Chem. Commun.*, 2013, **49**, 1297–1299.
- 2 Y. Zhang, J. Xu, P. Xu, Y. Zhu, X. Chen and W. Yu, *Nanotechnology*, 2010, **21**, 285501.
- 3 L. Lou, K. Yu, Z. Zhang, R. Huang, J. Zhu, Y. Wang and Z. Zhu, *Nano Res.*, 2012, **5**, 272–282.
- 4 Y. Luo, J. Luo, J. Jiang, W. Zhou, H. Yang, X. Qi, H. Zhang, H. J. Fan, Y. Denis and C. M. Li, *Energy Environ. Sci.*, 2012, **5**, 6559–6566.
- 5 J. Jiang, Y. Li, J. Liu, X. Huang, C. Yuan and X. W. D. Lou, *Adv. Mater.*, 2012, **24**, 5166–5180.
- 6 J. Li, S. K. Cushing, J. Bright, F. Meng, T. R. Senty, P. Zheng, A. D. Bristow and N. Wu, *ACS Catal.*, 2012, **3**, 47–51.
- 7 B. Lim, M. Jiang, P. H. C. Camargo, E. C. Cho, J. Tao, X. Lu, Y. Zhu and Y. Xia, *Science*, 2009, **324**, 1302–1305.
- 8 P. Massa, F. Ivorra, P. Haure and R. Fenoglio, *J. Hazard. Mater.*, 2011, **190**, 1068–1073.
- 9 X. Zhao, P. Wang and B. Li, *Chem. Commun.*, 2010, **46**, 6768–6770.
- 10 J. C. Park, A. Y. Kim, J. Y. Kim, S. Park, K. H. Park and H. Song, *Chem. Commun.*, 2012, **48**, 8484–8486.
- 11 Y. Feng, I. S. Cho, P. M. Rao, L. Cai and X. Zheng, *Nano Lett.*, 2012, **13**, 855–860.
- 12 S. I. In, D. D. Vaughn and R. E. Schaak, *Angew. Chem., Int. Ed.*, 2012, **51**, 3915–3918.
- 13 H. Xu, W. Wang and W. Zhu, *J. Phys. Chem. B*, 2006, **110**, 13829–13834.
- 14 M. Kaur, K. Muthe, S. Despande, S. Choudhury, J. Singh, N. Verma, S. Gupta and J. Yakhmi, *J. Cryst. Growth*, 2006, **289**, 670–675.
- 15 W. Wang, O. K. Varghese, C. Ruan, M. Paulose and C. A. Grimes, *J. Mater. Res.*, 2003, **18**, 2756–2759.
- 16 M. Cao, Y. Wang, C. Guo, Y. Qi, C. Hu and E. Wang, *J. Nanosci. Nanotechnol.*, 2004, **4**, 824–828.
- 17 J. Y. Kim, J. A. Rodriguez, J. C. Hanson, A. I. Frenkel and P. L. Lee, *J. Am. Chem. Soc.*, 2003, **125**, 10684–10692.
- 18 X. Jiang, T. Herricks and Y. Xia, *Nano Lett.*, 2002, **2**, 1333–1338.
- 19 L. Yuan, Y. Q. Wang, R. Mema and G. W. Zhou, *Acta Mater.*, 2011, **59**, 2491–2500.
- 20 R. Mema, L. Yuan, Q. T. Du, Y. Q. Wang and G. W. Zhou, *Chem. Phys. Lett.*, 2011, **512**, 87–91.
- 21 F. Hofer and P. Golob, *Ultramicroscopy*, 1987, **21**, 379–383.
- 22 R. Leapman, L. Grunes and P. Fejes, *Phys. Rev. B: Condens. Matter Mater. Phys.*, 1982, **26**, 614–635.
- 23 R. F. Egerton, *Electron energy-loss spectroscopy in the electron microscope*, Springer, New York, 2011.
- 24 D. F. Zhang, H. Zhang, L. Guo, K. Zheng, X. D. Han and Z. Zhang, *J. Mater. Chem.*, 2009, **19**, 5220–5225.
- 25 G. W. Zhou, L. Wang and J. C. Yang, *J. Appl. Phys.*, 2005, **97**, 063509.
- 26 L. Yuan, Q. Y. Yin, Y. Q. Wang and G. W. Zhou, *Chem. Phys. Lett.*, 2013, **590**, 92–96.
- 27 J. Shi, J. Li, X. Huang and Y. Tan, *Nano Res.*, 2011, **4**, 448–459.
- 28 H. Yu, J. Yu, S. Liu and S. Mann, *Chem. Mater.*, 2007, **19**, 4327–4334.
- 29 J. Bandara, I. Guasaquillo, P. Bowen, L. Soare, W. Jardim and J. Kiwi, *Langmuir*, 2005, **21**, 8554–8559.
- 30 T. Tatsuma, S. I. Tachibana, T. Miwa, D. A. Tryk and A. Fujishima, *J. Phys. Chem. B*, 1999, **103**, 8033–8035.